Available online at www.sciencedirect.com
ScienceDirect
Journal of Solid State Chemistry 179 (2006) 4011–4019
JOURNAL OF SOLID STATE CHEMISTRY
www.elsevier.com/locate/jssc

Structure refinement, dielectric, pyroelectric and Raman characterizations of $Ba_{1-x}La_{x(1-y)/2}Eu_{xy/2}Na_{x/2}TiO_3$ solid solution

Najmeddine Abdelmoula[a,*], Hamadi Khemakhem[a], Annie Simon[b], Mario Maglione[b]

[a]*Laboratoire des Matériaux Ferroélectriques, Faculté des Sciences de Sfax, BP 802, 3018 Sfax, Tunisia*
[b]*Institut de Chimie de la Matière Condensée de Bordeaux, ICMCB-CNRS Université Bordeaux I, 87, Avenue du Dr. A. Schweitzer, 33608 Pessac, France*

Received 29 June 2006; received in revised form 10 September 2006; accepted 12 September 2006
Available online 16 September 2006

Abstract

The perovskite-type oxides $Ba_{1-x}La_{x(1-y)/2}Eu_{xy/2}Na_{x/2}TiO_3$ ($0 \leqslant x \leqslant 0.5$ and $xy = 0.04$) were synthesized and characterized by X-ray diffraction as well as dielectric measurements and Raman spectroscopy. The crystal structure of these ceramics has been determined by the Rietveld refinement powder X-ray diffraction data at room temperature. These compounds crystallize at room temperature in tetragonal space group $P4mm$ for $0 \leqslant x \leqslant 0.1$ and in the cubic group $Pm\bar{3}m$ for $0.2 \leqslant x \leqslant 0.5$. The phase transition temperature T_C (or T_m) decreases as x content increases. The degree of diffuseness of the phase transition is more pronounced for higher x content, implying the existence of a composition-induced diffuse phase transition of the ceramics with $x \geqslant 0.1$. The evolution of the Raman spectra was studied as a function of various compositions at room temperature. The polarization state was checked by pyroelectric measurements.

Keywords: Ceramic; Rietveld refinement; Perovskite; Relaxor; Pyroelectric; Raman spectroscopy

1. Introduction

According to their behavior, the ferroelectric materials with perovskite-like structure may be divided into different classes depending on whether they are classical or relaxor ferroelectric [1]. Relaxor materials are characterized mainly by frequency dispersion and broad peaks in the dielectric susceptibility versus temperature [2]. Many investigations have been devoted to the study of the relaxation parameters in order to achieve their use in satisfactory capacitors and actuators [3]. The relaxor behavior was mainly obtained in lead-based ceramics for examples $PbMg_{1/3}Nb_{2/3}O_3$ and derived compounds [4,5]. However, these materials have a drawback due to the volatility and the toxicity of PbO. Up to now, current research is oriented to environment friendly applications using lead-free materials [6–8]. Ceramics based on barium titanate ($BaTiO_3$) are frequently used to manufacture multilayer ceramic capacitor and thermistors owing to their high dielectric constant [9]. Barium titanate ($BaTiO_3$) is the most common ferroelectric oxide in the perovskite ABO_3 structure [10]. In $BaTiO_3$ a phase transition occurs from rhombohedra (C_{3v}) to cubic (O_h) through orthorhombic (C_{2v}) and tetragonal (C_{4v}) as temperature increases to about 400 K. Each transition is a first-order transition [11]. Homovalent or heterovalent substitutions of barium or titanium ions were shown to give rise to various behaviors, including relaxor properties [12–17]. In addition, the aim for application was to prepare lead-free relaxor ceramics with such properties close to room temperature. In fact, up to now, lead-free relaxor presented value of T_m often widely lower than room temperature [18]. The present report is aimed as designing and characterizing new lead-free ferroelectric relaxors derived from $BaTiO_3$. We investigate the system $Ba_{1-x}La_{x(1-y)/2}Eu_{xy/2}Na_{x/2}TiO_3$ ($0 \leqslant x \leqslant 0.5$), the Eu content will be fixed at 0.02. In our previous work we have reported that the heterovalent substitution of barium by La^{3+}, Na^{+}, and Eu^{3+} exhibit relaxor properties [19]. The purpose of this paper is to study the structure refinement, the diffuse phase transition behavior and the pyroelectric and Raman scattering

*Corresponding author. Fax: +216 74 274 437.
E-mail address: najmeddine.abdelmoula@fss.rnu.tn (N. Abdelmoula).

0022-4596/$ - see front matter © 2006 Elsevier Inc. All rights reserved.
doi:10.1016/j.jssc.2006.09.006

characterizations for all compositions of the system $Ba_{1-x}La_{x(1-y)/2}Eu_{xy/2}Na_{x/2}TiO_3$ in the classical and relaxor regions for $0 \leqslant x < 0.1$ and $0.1 \leqslant x \leqslant 0.5$, respectively, which are separated in our previous work [19].

2. Experimental procedure

$Ba_{1-x}La_{x(1-y)/2}Eu_{xy/2}Na_{x/2}TiO_3$ ($0 \leqslant x \leqslant 0.5$ and xy is fixed at 0.04 in the solution) polycrystalline ceramic specimens were prepared by conventional standard solid state synthesis technique. $BaCO_3$ (99.98%), La_2O_3 (99.99%), Eu_2O_3 (99.99%), Na_2CO_3 (99.98%) and TiO_2 (99.98%) powders were used. In order to evaporate H_2O, these oxides were dried at 393 K for 15 h before weighing. The mixture was ball-milled in ethanol for 1 h, dried and then calcined in pure oxygen atmosphere at 1373 K for 12 h to achieve de-carbonation. The obtained material was then ball-milled again with de-ionized water added of appropriate amount of dispersing agent for 1 h. After drying, the powder was pressed into pellets of 8 mm in diameter and about 1 mm thickness under 100 MPa. These pellets were sintered in pure oxygen atmosphere at 1593 K for 3 h and finally, these pellets were furnace cooled to room temperature. Powder X-ray diffraction at room temperature was performed on a Philips diffractometer equipped with curved Ge crystal monochromator using Cu$K\alpha$ radiation ($\lambda = 1.5406$ Å). Data were collected in the range of $10^\circ \leqslant 2\theta \leqslant 110^\circ$, with 0.02° step and 10 s counting time. Data were analyzed by Rietveld method [20] using the FULLPROF program [21]. The peak shape was described by a pseudo-voigt function and the background level was defined by a polynomial function. The refined parameters were background coefficients, scale factor, lattice parameters, atomic positions and the counter zero point.

The diameter shrinkage, Φinit$-\Phi$final/Φinit, and the compactness (experimental density/theoretical density) were systematically determined. Their values were in the range 0.13–0.15, 0.92 and 0.95, respectively.

3. Results and discussion

3.1. Structure analysis

The powder X-ray diffraction patterns at room temperature of $Ba_{1-x}La_{x(1-y)/2}Eu_{xy/2}Na_{x/2}TiO_3$ ($xy = 0.04$) were indexed in tetragonal perovskite-type structure with space group $P4mm$ like $BaTiO_3$ [22] for $x \leqslant 0.1$. For $x \geqslant 0.2$, all of the diffraction lines were assigned in cubic structure with $Pm\bar{3}m$ space group. This analysis shows that all compositions are in pure perovskite phase and with good homogeneity.

The structure refinement was carried out by Rietveld analysis of the XRD data. As examples Figs. 1 and 2 show the observed and calculated XRD patterns of $Ba_{1-x}La_{x(1-y)/2}Eu_{xy/2}Na_{x/2}TiO_3$ for $x = 0.05$ and 0.35. After initial refinement of background, zero point, unit cell parameters and profile parameters [19], the positional atomic parameters, the occupancy factors and thermal parameters were refined. Crystallographic parameters and the final positional and occupancy factors of $Ba_{1-x}La_{x(1-y)/2}Eu_{xy/2}Na_{x/2}TiO_3$ are summarized in Tables 1 and 2. The refined occupancy factors are in good agreement with those experimentally estimated. The cell parameters decrease with increasing x. The ionic radii of the Ba^{2+}, La^{3+}, Eu^{3+} and Na^{+} ions in eight coordination

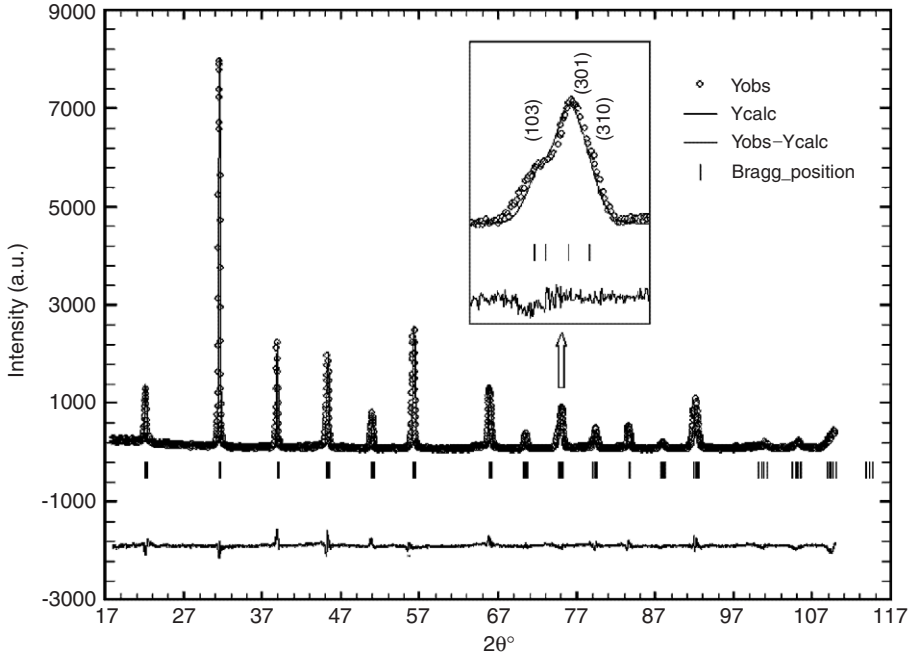

Fig. 1. Observed, calculated and difference X-ray diffraction patterns of $Ba_{0.95}La_{0.005}Eu_{0.02}Na_{0.025}TiO_3$ ($x = 0.05$) in the space group $P4mm$.

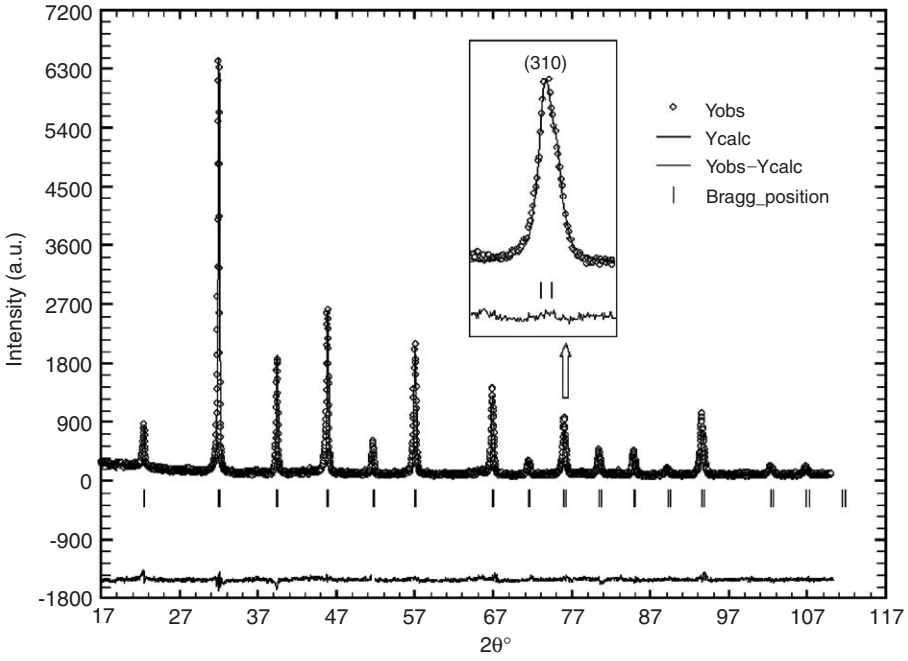

Fig. 2. Observed, calculated and difference X-ray diffraction patterns of $Ba_{0.65}La_{0.155}Eu_{0.02}Na_{0.175}TiO_3$ ($x = 0.35$) in the space group $Pm\bar{3}m$.

Table 1
Refined structure parameters at room temperature for the tetragonal region $x \leqslant 0.1$ and $xy = 0.04$ with space group $P4mm$

Sample	Lattice and refinement parameters	Atomic parameters				
		Atom	x	y	z	Occ.
$x = 0.05$	$a = 3.9989(9)$ (Å)	Ba	0	0	0	0.1187(4)
	$c = 4.0181(1)$ (Å)	Na	0	0	0	0.0031(1)
	$V = 64.2571(3)$ (Å^3)	La	0	0	0	0.0006(1)
	$R_p = 6.07$	Eu	0	0	0	0.0025(1)
	$R_{wp} = 7.93$	Ti	0.5	0.5	0.4853(5)	0.1250(1)
	$\chi^2 = 4.12$	O1	0.5	0	0.5091(7)	0.2500(2)
		O2	0.5	0.5	0.0021(1)	0.1250(1)
$x = 0.08$	$a = 3.9961(2)$ (Å)	Ba	0	0	0	0.1150(2)
	$c = 4.0167(5)$ (Å)	Na	0	0	0	0.0050(1)
	$V = 64.1433(8)$ (Å^3)	La	0	0	0	0.0024(9)
	$R_p = 5.29$	Eu	0	0	0	0.0025(1)
	$R_{wp} = 6.73$	Ti	0.5	0.5	0.4835(2)	0.1250(2)
	$\chi^2 = 3.57$	O1	0.5	0	0.4947(3)	0.2500(1)
		O2	0.5	0.5	0.0079(1)	0.1250(1)
$x = 0.10$	$a = 3.9939(1)$ (Å)	Ba	0	0	0	0.1124(9)
	$c = 4.0105(8)$ (Å)	Na	0	0	0	0.0062(3)
	$V = 63.9740(3)$ (Å^3)	La	0	0	0	0.0037(3)
	$R_p = 7.75$	Eu	0	0	0	0.0025(0)
	$R_{wp} = 4.49$	Ti	0	0.5	0.4983(7)	0.1250(2)
	$\chi^2 = 3.63$	O1	0.5	0	0.5187(7)	0.2499(7)
		O2	0.5	0.5	0.0027(5)	0.1249(1)

are 1.42, 1.16, 1.004 and 1.18 Å, respectively [23]. Therefore, it is obvious that an increase in the cell constants responds to the difference in the ionic radii between Ba^{2+} and $La^{3+}/Na^{+}/Eu^{3+}$ ions.

In tetragonal perovskite-type $Ba_{1-x}La_{x(1-y)/2}Eu_{xy/2}Na_{x/2}TiO_3$ (for $x \leqslant 0.1$ and $xy = 0.04$), A site cations (Ba, La, Na and Eu) coordinate with 12 anions: 4 O(1) and 8 O(2) ions and B site cations (Ti ions) coordinate with 6 anions: 4 O(1) and 2 O(2). In cubic perovskite-type $Ba_{1-x}La_{x(1-y)/2}Eu_{xy/2}Na_{x/2}TiO_3$ (for $x \geqslant 0.2$ and $xy = 0.04$) A site cations are coordinated by 12 oxygen ions and Ti ion is surrounded by six oxygen ions making regular octahedra (TiO_6). Table 3 shows

Table 2
Refined structure parameters at room temperature for the cubic region $x \geqslant 0.2$ and $xy = 0.04$ with space group $Pm\bar{3}m$

Sample	Lattice and refinement parameters	Atomic parameters				
		Atom	x	y	z	Occ.
$x = 0.20$	$a = 3.9837(1)$ (Å)	Ba	0	0	0	0.0166(4)
	$V = 63.2212(6)$ (Å^3)	Na	0	0	0	0.0020(5)
	$R_p = 5.15$	La	0	0	0	0.0016(3)
	$R_{wp} = 6.47$	Eu	0	0	0	0.0004(1)
	$\chi^2 = 3.87$	Ti	0.5	0.5	0.5	0.0208(3)
		O	0.5	0	0.5	0.0625(1)
$x = 0.30$	$a = 3.9701(2)$ (Å)	Ba	0	0	0	0.0145(7)
	$V = 62.5764(4)$ (Å^3)	Na	0	0	0	0.0031(1)
	$R_p = 5.62$	La	0	0	0	0.0002(5)
	$R_{wp} = 4.91$	Eu	0	0	0	0.0004(2)
	$\chi^2 = 3.15$	Ti	0.5	0.5	0.5	0.0208(1)
		O	0.5	0	0.5	0.0624(9)
$x = 0.35$	$a = 3.9633(9)$ (Å)	Ba	0	0	0	0.0135(2)
	$V = 62.2587(5)$ (Å^3)	Na	0	0	0	0.0036(5)
	$R_p = 5.68$	La	0	0	0	0.0032(3)
	$R_{wp} = 5.36$	Eu	0	0	0	0.0004(2)
	$\chi^2 = 2.99$	Ti	0.5	0.5	0.5	0.0208(2)
		O	0.5	0	0.5	0.0625(1)
$x = 0.40$	$a = 3.9569(1)$ (Å)	Ba	0	0	0	0.0124(7)
	$V = 61.9538(8)$ (Å^3)	Na	0	0	0	0.0041(5)
	$R_p = 5.47$	La	0	0	0	0.0037(3)
	$R_{wp} = 5.36$	Eu	0	0	0	0.0004(1)
	$\chi^2 = 2.41$	Ti	0.5	0.5	0.5	0.0208(1)
		O	0.5	0	0.5	0.0625(0)
$x = 0.45$	$a = 3.9497(9)$ (Å)	Ba	0	0	0	0.0114(5)
	$V = 61.6200(4)$ (Å^3)	Na	0	0	0	0.0046(5)
	$R_p = 4.87$	La	0	0	0	0.0042(3)
	$R_{wp} = 4.56$	Eu	0	0	0	0.0004(1)
	$\chi^2 = 2.85$	Ti	0.5	0.5	0.5	0.0208(1)
		O	0.5	0	0.5	0.0624(9)
$x = 0.50$	$a = 3.9411(3)$ (Å)	Ba	0	0	0	0.0103(8)
	$V = 61.2156(2)$ (Å^3)	Na	0	0	0	0.0051(9)
	$R_p = 4.56$	La	0	0	0	0.0047(7)
	$R_{wp} = 4.23$	Eu	0	0	0	0.0004(0)
	$\chi^2 = 2.57$	Ti	0.5	0.5	0.5	0.0208(1)
		O	0.5	0	0.5	0.0624(8)

Table 3
Distances (Å) and angles (deg) between the oxygen atom and the titanium atom from the powder X-ray diffraction data for $Ba_{1-x}La_{x(1-y)/2}Eu_{xy/2}Na_{x/2}TiO_3$ ($0 \leqslant x \leqslant 0.5$ and $xy = 0.04$)

Sample	Ti–O1	Ti–O2	Ti–O1–Ti	Ti–O2–Ti
$x = 0.05$	1.9994(9)	2.0090(5)	167.7621(1)	180
$x = 0.08$	1.9980(6)	2.0083(7)	175.2403(3)	180
$x = 0.10$	1.9969(5)	2.0052(9)	179.9740(5)	180
$x = 0.20$	1.9918(5)	1.9918(5)	180	180
$x = 0.30$	1.9850(5)	1.9850(5)	180	180
$x = 0.35$	1.9817(2)	1.9817(1)	180	180
$x = 0.40$	1.9784(5)	1.9784(5)	180	180
$x = 0.45$	1.9749(1)	1.9749(3)	180	180
$x = 0.50$	1.9705(5)	1.9705(5)	180	180

the various Ti–O distances and Ti–O–Ti angles calculated from the atomic coordinates obtained by the Rietveld refinements. The cell parameters and unit cell volume decrease with increasing x, the Ti–O distances also decrease as x increases. Although for $x \leqslant 0.1$, the Ti–O(1)–Ti, angle are less than 180° and increase with increasing x. Therefore, replacement of Ba by (La, Eu and Na) introduce a smaller A site ions and causes a decrease in space between network of TiO_6 octahedra and consequently in the unit cell volume.

3.2. Dielectric properties

Dielectric measurements were performed on ceramic disks. Before measurements, gold electrodes were deposited

on polished pellets by cathodic sputtering. The variation of permittivity as a function of both temperature and frequency was determined using a Wayne-Kerr 6425 component analyzer.

Fig. 3 shows the dielectric permittivity ε'_r as a function of temperature at 1 kHz for $Ba_{1-x}La_{x(1-y)/2}Eu_{xy/2}Na_{x/2}TiO_3$ samples with $0 \leqslant x \leqslant 0.45$ and $xy = 0.04$. Several remarked variations are observed due to substitution of Ba^{2+} by La^{3+}, Eu^{3+} and Na^{+}. Only one peak was observed corresponding to the phase transition of paraelectric (cubic)-ferroelectric (tetragonal) at T_C. Temperature of dielectric maximum (T_m) decreases with x indicating La^{3+}, Eu^{3+} and Na^{+} have entered into lattice. In addition, with the increase of x, dielectric peak become broader, meanwhile dielectric maximum decrease monotonically. One of the principal parameters determining the phase transitions and related physical properties for the crystalline materials possessing the oxygen octahedral is a non-stoichiometric cationic substitution, which may cause additional increase of an-harmonic electron–phonon interactions responsible for the phase transitions, that it was shown for niobates [24].

It can see from Fig. 3 and Table 3 that T_m decreases when the average of Ti–O distance decreases. This result shows that substituting Ba by (La, Eu and Na) introduces a smaller A site ions which lead the polarization of titanium ions in the TiO_6 octahedra to becomes smaller. A similar behavior was observed in the system $(Ln_{1/2}Na_{1/2})TiO_3$ (Ln = Dy, Ho, Er, Tm, yb, Lu) [25].

It is known that for a normal ferroelectric, the dielectric constant above the Curie point follows the Curie–Weiss law described by

$$\varepsilon'_r = \frac{C}{T - T_0} \quad (T > T_C), \tag{1}$$

where C is the Curie–Weiss constant and T_0 is the Curie–Weiss temperature. Fig. 4 shows the inverse ε'_r as a function of temperature at 1 kHz and the fits to the experimental data by Eq. (1). The parameters obtained from the fitting are listed in Table 4. It was found that for the samples with lower composition x, the dielectric constant obeys the Curie–Weiss law. However, for $x > 0.1$, a deviation from the Curie–Weiss law is deduced. A similar behavior was observed in 0.9PMN–0.1PT–x%Ca [26] and (Ba,Sr)(Zr,Ti)O_3 [27].

A parameter, ΔT_m, is defined to describe the deviation degree of ε'_r from the Curie–Weiss law as follows:

$$\Delta T_m = T_{dev} - T_m, \tag{2}$$

where T_{dev} denotes the temperature from which ε'_r starts to deviate from the Curie–Weiss law and T_m represents the temperature of permittivity maximum. The values of ΔT_m increase with increasing x, which further provides the evidence of a composition-induced diffuse phase transition behavior in the $Ba_{1-x}La_{x(1-y)/2}Eu_{xy/2}Na_{x/2}TiO_3$ ceramics with $0 \leqslant x \leqslant 0.45$ and $xy = 0.04$.

A modified empirical expression was proposed by Uchino and Nomura [28] to describe the diffuseness of the phase transition temperature:

$$\frac{1}{\varepsilon'_r} - \frac{1}{\varepsilon'_{rm}} = \frac{(T - T_m)^\gamma}{C'}, \tag{3}$$

where γ and C' are assumed to be constants, and the γ value is between 1 and 2. The parameter γ gives information on the character of the phase transition and only depending on the composition of the specimens. The limiting values $\gamma = 1$ and 2 reduce the equation to Curie–Weiss law for the case of normal ferroelectric and the quadratic for an ideal relaxor ferroelectric, respectively [29].

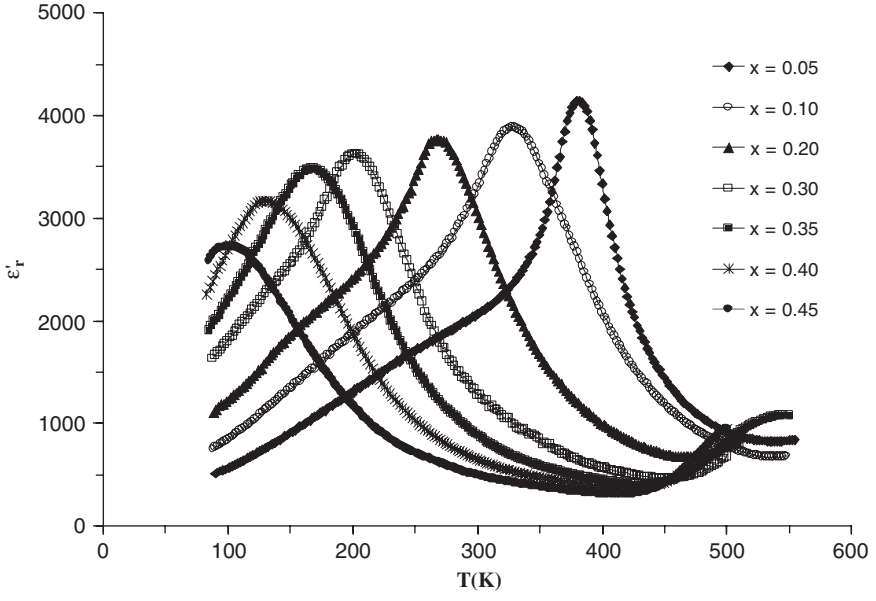

Fig. 3. Temperature dependence of dielectric permittivity of $Ba_{1-x}La_{x(1-y)/2}Eu_{xy/2}Na_{x/2}TiO_3$ ($0 \leqslant x \leqslant 0.45$ and $xy = 0.04$) ceramics at 1 kHz.

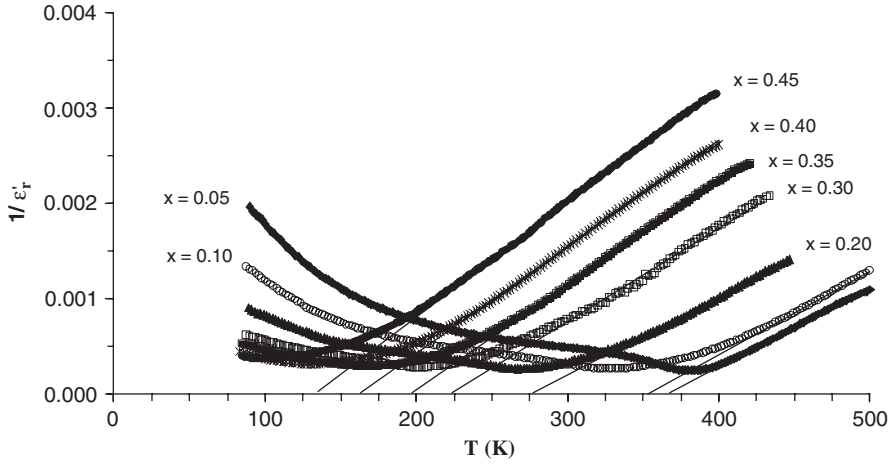

Fig. 4. The temperature dependence of $1/\varepsilon'_r$ at 1 kHz for $Ba_{1-x}La_{x(1-y)/2}Eu_{xy/2}Na_{x/2}TiO_3$ ($0 \leqslant x \leqslant 0.45$ and $xy = 0.04$) ceramics and the fit to Curie–Weiss law. (The symbols: experimental data; the solid line: fitting curves.)

Table 4
The temperature of permittivity maximum (T_m), the Curie–Weiss temperature (T_0), the Curie–Weiss constant (C), the temperature above which the permittivity follows the Curie–Weiss (T_{dev}), $\Delta T_m = T_{dev} - T_m$ and the diffuseness coefficient (γ) for $Ba_{1-x}La_{x(1-y)/2}Eu_{xy/2}Na_{x/2}TiO_3$ ceramics at 1 kHz

Compositions	T_m (K)	T_0 (K)	C (10^5 K)	T_{dev} (K)	ΔT_m (K)	γ
$x = 0.05$	384	370	1.207	390	6	1.43
$x = 0.08$	366	358	1.138	374	8	1.51
$x = 0.10$	334	353	1.143	354	20	1.68
$x = 0.20$	268	278	1.22	326	58	1.75
$x = 0.30$	200	224	1.012	292	92	1.85
$x = 0.35$	164	197	0.911	264	100	1.95
$x = 0.40$	128	165	0.891	238	110	1.97
$x = 0.45$	100	135	0.831	221	121	1.99

The plots of $\log(1/\varepsilon'_r - \varepsilon'_{rm})$ as a function of $\log(T–T_m)$ for $Ba_{1-x}La_{x(1-y)/2}Eu_{xy/2}Na_{x/2}TiO_3$ ($0 \leqslant x \leqslant 0.45$ and $xy = 0.04$) are shown in Fig. 5. A linear relationship is observed for all samples. The slope of the fitting curves is used to determine the value of γ. The γ value varies from 1.43 to 1.99 as x increases from 0.05 to 0.45, respectively (Table 4), indicating that a normal ferroelectric $BaTiO_3$ changes to a relaxor ferroelectric by doping of La, Na and Eu ions. According to our previous work [19], it can be noted that for $\gamma \geqslant 1.68$, the ceramic ($x = 0.1$) exhibit features of diffuse phase transition and relaxor ferroelectric behavior. This phenomenon has been found in many compounds such as $Pb(Mg_{1/3}Nb_{2/3})O_3$–$Pb(Ni_{1/3}Nb_{2/3})O_3$–($PbTiO_3$) system [30] and $(Na_{0.5}K_{0.5})NbO_3$–$SrTiO_3$ ceramics [31]. The relaxor behavior can be induced by many reasons such as microscopic regions into macropolar regions, or coupling of the order parameter and local disorder mode through the local strain. In our solid solution Ba, La, Na and Eu ions occupy the A sites of ABO_3 perovskite structure, therefore the cation disorder in perovskite unit cell should be one of the reason for the appearance of relaxor state. On the other hand, the macrodomains in pure $BaTiO_3$ should be divided into microdomains with increasing the La and Na ions doping, which also may result in the appearance of the relaxor behavior.

3.3. Pyroelectric properties

The ceramic sample $Ba_{0.90}La_{0.03}Eu_{0.02}Na_{0.05}TiO_3$ ($x = 0.1$ and $xy = 0.04$) was poled using a dc electric field of 1.1 kV/cm at 377 K for 10 min and then short circuited for several hours in order to eliminate any residual space charge. The pyroelectric current was measured on heating at a rate of about 2.2 K/min from 100 to 370 K. The temperature dependence of the pyroelectric coefficient (p) was calculated from the rate of variation of the temperature b and pyroelectric current i following the relation $p = i/(sb)$, where s is the area of an electrode. The spontaneous polarization P_S was calculated by integration of the value of p versus T. The results are shown in Fig. 6. The pyroelectric coefficient, p, shows a broad peak which is characteristic of the ferroelectric–paraelectric phase transition at a temperature around T_m for the composition $x = 0.1$. The spontaneous polarization, P_S, presents a constant value at low temperature and then decreases progressively to attain zero at a temperature $T_m + 40$ K. A similar behavior was observed in $Ba_{1-3a}Bi_{2a}TiO_3$ system [32]. This behavior is not only linked to the order type of the transition but also to the diffuse character of the phase transition.

3.4. Raman scattering

Raman scattering experiments were done using a Dilor Z24 triple monochromator. The spectral resolution was 3 cm^{-1}. The excitation light was the 514.5 nm line of an argon ion laser.

In its high temperature cubic phase, barium titanate has the perovskite cubic structure. Using a standard group

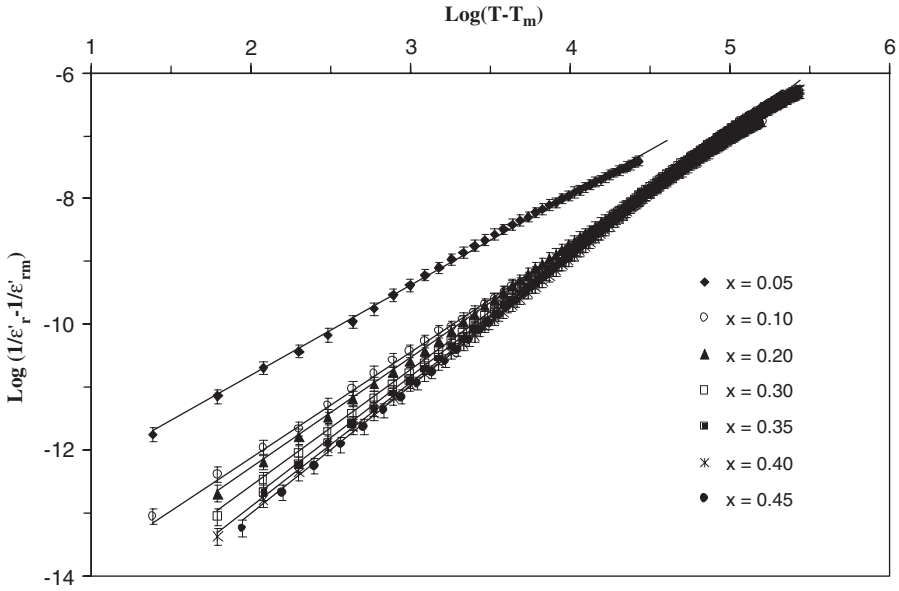

Fig. 5. Plot of $\log(1/\varepsilon'_r - \varepsilon'_{rm})$ as a function of $\log(T–T_m)$ for the $Ba_{1-x}La_{x(1-y)/2}Eu_{xy/2}Na_{x/2}TiO_3$ ($0 \leqslant x \leqslant 0.45$ and $xy = 0.04$) ceramics. (The symbols: experimental data; the solid line: fitting to Eq. (3).)

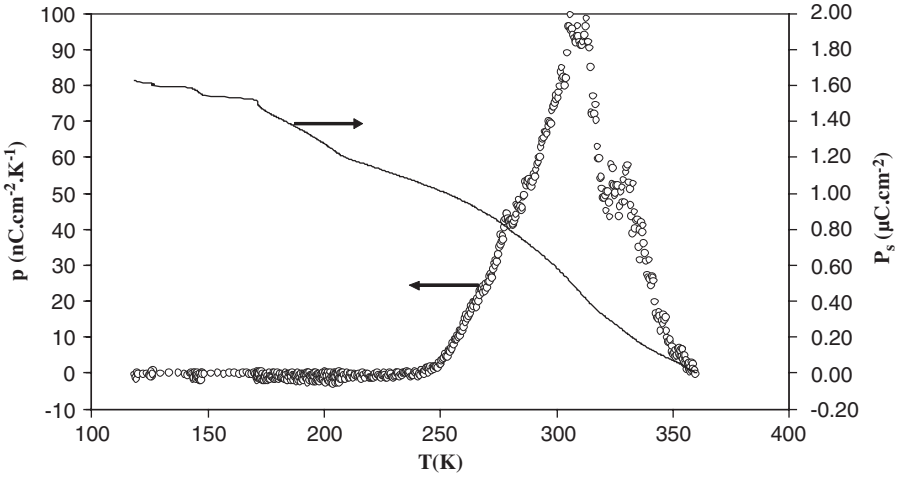

Fig. 6. Temperature dependence of the spontaneous polarization P_S and the pyroelectric coefficient p for the ceramic composition $Ba_{0.90}La_{0.03}Eu_{0.02}Na_{0.05}TiO_3$ ($x = 0.1$ and $xy = 0.04$).

theory analysis, normal optic modes can be shown to belong to the 3 $F_{1u} \oplus F_{2u}$ irreducible representations of the point group O_h. When entering the tetragonal C_{4v} phase, the IR active F_{1u} modes are expected to split into $A_1 \oplus E$, and the silent mode F_{2u} into $B_1 \oplus E$ [33].

The Raman spectra of several compositions at room temperature of the $Ba_{1-x}La_{x(1-y)/2}Eu_{xy/2}Na_{x/2}TiO_3$ system are given in Fig. 7. It can be noted that in the region 210–310 cm^{-1}, the spectra of samples with compositions $x \leqslant 0.1$ are different to the other spectra corresponding to $x \geqslant 0.2$. This result confirms the structural transition from tetragonal to cubic symmetry obtained by X-ray diffraction analyses. When x content increases all the bands show significant broading, a weaker intensity and shifted to the high frequency. This would be undoubtedly connected with the disorder created on the A site of $BaTiO_3$ as a consequence of La/Na/Eu substitution. Comparing our data to published results by Kchikech and Maglione [34], Lagos et al. [35] and Kim et al. [36] on the tetragonal $BaTiO_3$, we are able to make the following normal mode assignments. For $x \leqslant 0.1$, the A_1 transverse optical (TO) modes are observed as broad lines at 250 and 522 cm^{-1}. The A_1 longitudinal optical (LO) modes can be identified at 725 cm^{-1}. The 307 cm^{-1} peak can be assigned to the $E(TO + LO) + B_1$ modes [35]. This mode appears only on entering the tetragonal phase and can be therefore considered as the signature of the tetragonal to cubic phase transition. The spectra corresponding to $x = 0.20$ exhibit a small shoulder at the frequency of the $E(TO + LO) + B1$ mode. Since, Raman spectroscopy is more

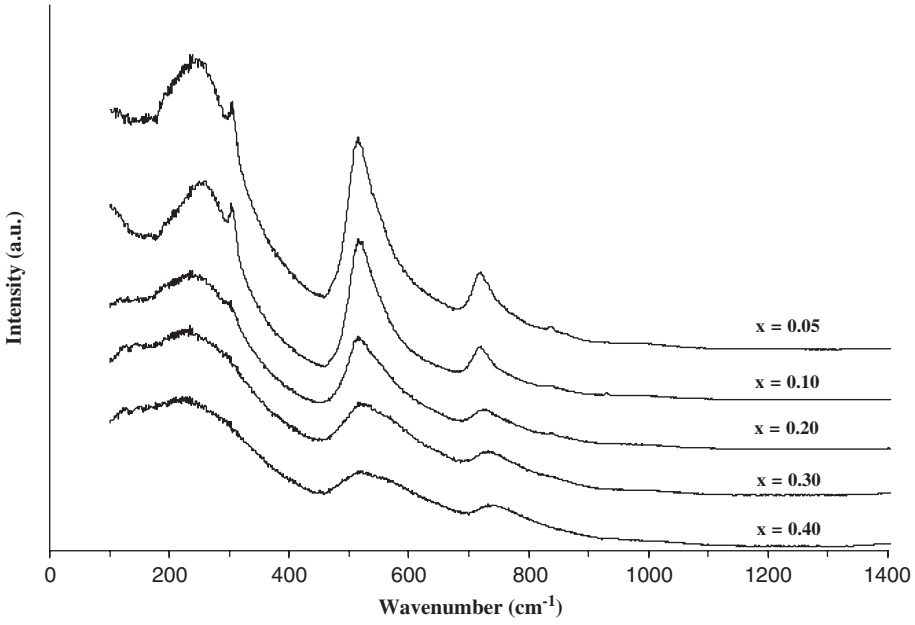

Fig. 7. Raman spectra of several compositions of the $Ba_{1-x}La_{x(1-y)/2}Eu_{xy/2}Na_{x/2}TiO_3$ ($0 \leqslant x \leqslant 0.5$ and $xy = 0.04$) system.

sensitive than X-ray diffraction to the local distortion of the oxygen octahedra; it may suggest a coexistence of the tetragonal and cubic phases. This effect can be easily explained because the phase transition of the sample with $x = 0.2$ is just below room temperature and has an important diffuse character. The cubic paraelectric phase is characterized by three very broad line at $\approx$240, 525 and 745 cm^{-1}. It should be pointed out that normal modes are not Raman active in the paraelectric phase and the origin of their activation should be found in a strong disorder. In addition, according to the literature [37], the low frequency band was assigned to vibration within the A site of the perovskite, whereas the higher frequency bands can probably be assigned to vibrations of the TiO_6 octahedra.

4. Conclusion

Ceramics derived from $BaTiO_3$ by substitution of Ba^{2+} cation by La^{3+}, Eu^{3+} and Na^{+} cations have been investigated by several physical experiments. The crystal structure of $Ba_{1-x}La_{x(1-y)/2}Eu_{xy/2}Na_{x/2}TiO_3$ ($0 \leqslant x \leqslant 0.5$ and $xy = 0.04$) materials has been refined by the Rietveld method from X-ray powder diffraction data. A structural phase transition from tetragonal to cubic systems was observed for $0.1 \leqslant x \leqslant 0.2$. The degree of diffuseness of the phase transition is more pronounced for higher x content, implying the existence of a composition-induced diffuse phase transition of the ceramics with $x \geqslant 0.1$. The evolution of pyroelectric coefficient shows the presence of the ferroelectric–paraelectric phase transition for the composition $x = 0.1$; the variation of P_S with temperature characterizes the relaxor character in this composition. The evolution of the Raman spectra at room temperature for various compositions confirms our structural and dielectrics results.

Acknowledgment

The authors would kindly like to thank Prof. Michel Couzi for Raman spectroscopy analysis of the samples.

References

[1] L.E. Cross, Ferroelectrics 76 (1987) 241.
[2] L.E. Cross, Ferroelectrics 151 (1994) 305.
[3] K. Uchino, Ferroelectrics 151 (1994) 321.
[4] N. Setter, L.E. Cross, J. Appl. Phys. 51 (1980) 4356.
[5] X. Yao, Z.L. Chen, L.E. Cross, J. Appl. Phys. 54 (1984) 3399.
[6] A. Aydi, H. Khemakhem, C. Boudaya, R. Von Der Mühll, A. Simon, Solid State Sci. 6 (2004) 333.
[7] H. Abdelkefi, H. Khemakhem, G. Velu, J.C. Carru, R. Von Der Mühll, J. Alloys Compd. 399 (2005) 1.
[8] W. Sakamoto, Y. Masuda, T. Yogo, J. Alloys Compd. 408 (2006) 543.
[9] Y. Wang, L. Li, J. Qi, Z. Gui, Int. Ceram. J. 28 (2002) 657.
[10] M.E. Lines, A.M. Glass, Principles and Applications of Ferroelectrics and Related Materials, Oxford University Press, Oxford, 1977.
[11] S. Komine, E. Iguchi, J. Phys.: Condens. Matter 14 (2002) 8445.
[12] J. Ravez, A. Simon, J. Korean Phys. Soc. 32 (1998) S955.
[13] J. Ravez, A. Simon, Eur. Phys. J. Appl. Phys. 11 (2000) 9.
[14] H. Khemakhem, A. Simon, R. Von Der Mühll, J. Ravez, J. Phys.: Condens. Matter 12 (2000) 5951.
[15] S. Komine, E. Iguchi, J. Phys.: Condens. Matter 14 (2002) 2043.
[16] F. Bahri, A. Simon, H. Khemakhem, J. Ravez, Phys. Status Solidi (a) 184 (2001) 459.
[17] N. Abdelmoula, H. Chaabane, H. Khemakhem, R. Von der Mühll, A. Simon, Phys. Status Solidi (a) 203 (2006) 987.
[18] J. Ravez, A. Simon, J. Solid State Chem. 162 (2001) 260.
[19] N. Abdelmoula, H. Khemakhem, R. Von der Mühll, A. Simon, J. Alloys Compd. 417 (2006) 264.
[20] H.M. Rietveld, J. Appl. Crystallogr. 2 (1969) 65.

[21] J. Rodriguez-Carvajal, Program Fullprof, Laboratoire Léon Brillouin, (CEA-CNRS), Version 3.5d, LLB-JRC, 1998.
[22] H.H. Weider, Phys. Rev. 99 (1955) 1161.
[23] R.D. Shannon, Acta Crystallogr. A 32 (1976) 751.
[24] I.V. Kityk, M. Makowska-Janusik, M.D. Fontana, M. Aillerie, A. Fahmi, J. Appl. Phys. 90 (2001) 5542.
[25] Y.J. Shan, T. Nakamura, Y. Inaguma, M. Itoh, Solid State Ion. 108 (1998) 123.
[26] N. Zhong, W. Yao, P. Xiang, C. Feng, S. Kojima, Solid State Commun. 134 (2005) 425.
[27] X.G. Tang, X.X. Wang, K.-H. Chew, H.L.W. Chan, Solid State Commun. 136 (2005) 89.
[28] K. Uchino, S. Nomura, Ferroelectr. Lett. Sec. 44 (1982) 55.
[29] D. Viehland, M. Wuttig, L.E. Cross, Ferroelectrics 120 (1991) 71.
[30] C. Lei, K. Chen, X. Zhang, Mater. Sci. Eng. B 111 (2004) 107.
[31] Y. Guo, K.I. Kakimoto, H. Ohsato, Solid State Commun 129 (2004) 279.
[32] F. Bahri, H. Khemakhem, A. Simon, R. Von Der Mühll, J. Ravez, Solid State Sci. 5 (2003) 1235.
[33] R. Farhi, M. El Marssi, A. Simon, J. Ravez, Eur. Phys. J. B 9 (1999) 599.
[34] M. Kchikech, M. Maglione, J. Phys.: Condens. Matter 6 (1994) 10159.
[35] L.P. Lagos, Z.R. Hermans, N. Velasco, G. Tarrach, F. Schlaphof, C. Loppacher, L.M. Eng, Surf. Sci. 532 (2003) 493.
[36] Y. Kim, J.K. Jung, K. Ryu, Mater. Res. Bull. 39 (2004) 1045.
[37] B. Güttlera, B. Mihailovab, R. Stoscha, U. Bismayerc, M. Gospodinovd, J. Mol. Struct. 661 (2003) 469.